IEEE Access
Multidisciplinary | Rapid Review | Open Access Journal

Received October 13, 2017, accepted December 20, 2017, date of publication January 8, 2018,
date of current version February 28, 2018.

Digital Object Identifier 10.1109/ACCESS.2018.2790482

Multi-Semi-Couple Super-Resolution Method for Edge Computing

XIAOMIN YANG[1], WEI WU[1], KAI LIU[2], (Senior Member, IEEE), PYOUNG WON KIM[3], ARUN KUMAR SANGAIAH[4], AND GWANGGIL JEON[5], (Member, IEEE)

[1]College of Electronics and Information Engineering, Sichuan University, Chengdu 610064, China
[2]School of Electrical Engineering and Information, Sichuan University, Chengdu 610064, China
[3]Department of Korean Language Education, Incheon National University, Incheon 22012, South Korea
[4]School of Computing Science and Engineering, VIT University, Vellore 632014, India
[5]Department of Embedded Systems Engineering, Incheon National University, Incheon 22012, South Korea

Corresponding author: Wei Wu (wuwei@scu.edu.cn)

This work was supported in part by the National Natural Science Foundation of China under Grant 61701327, Grant 61711540303, and Grant 61473198, in part by the National Research Foundation of Korea under Grant NRF-2017K2A9A2A06013711, and in part by the Priority Academic Program Development of Jiangsu Higher Education Institutions Fund, Jiangsu Collaborative Innovation Center on Atmospheric Environment and Equipment Technology.

ABSTRACT Video analyses based on edge computing typically need high-resolution video images, while, in practice, the resolutions of captured video images may not high enough. Thus, super-resolution techniques are possible solutions for such purpose with input low-resolution images. Sparse-coding-based super-resolution methods are well known for their efficiency. However, the current sparse-coding-based methods suffer from two major problems. First, the sparse coefficient of a low-resolution patch is assumed to be same as the sparse coefficient of its corresponding high-resolution patch, which is too strict to deal with various patterns; and second, the current methods only learn one pair of high-resolution and low-resolution dictionaries, while, since patches in image are of diversity in real world, it is difficult to use only one pair of dictionaries to cover all possible patches. In this paper, to overcome these two issues, we propose a super-resolution method to: 1) relax the assumption by linearizing the sparse coefficient of a low-resolution patch to that of high-resolution patch and 2) minimize super-resolution errors by jointly partitioning training patches into several clusters and learning dictionaries. Experimental results validate that our algorithm achieve more faithful reconstructions.

INDEX TERMS Edge computing, super-resolution, spare coding.

I. INTRODUCTION

Smart phone cameras as well as network cameras are deployed everywhere in the world. Images and videos are generated every time. It is heavy load for cloud computing if all data is directly uploaded. Therefore, preprocessing data at the edge devices will greatly help to reduce network load. Edge computing refers to processing/preprocessing videos/images at the edge of networks. Edge devices can be any available computing resources, e.g., smart phone, gateway, etc. However, because of limitation of hardware, the resolutions of images don't meet requirements.

Super-resolution (SR) methods are effective for obtaining high resolution (HR) images from low-resolution (LR) images. Thus, it is necessary to exploit SR methods to increase the resolutions of images at edge devices. Fig. 1 illustrates the architecture of edge computing for video analyses. In Fig. 1, cameras capture LR images, and upload them to edge devices. To reduce the network load, edge devices increase the resolutions of the images and then analyze the SR images.

This study focuses on an SR method for edge computing. Currently, there are three categories of SR methods, and they are interpolation-based methods [1], [2], multiframe-based methods [3]–[5] and learning-based methods [6]–[18].

Interpolation-based methods utilize the information of neighboring pixels to estimate HR pixels. However, given that interpolations cannot bring any new details into reconstructed images, these methods suffer from producing blurred edges and artifacts.

Multiframe-based methods [3]–[5] need several LR images obtained from the same scene with slightly-moved viewpoints. Multiframe-based SR methods reconstruct HR image

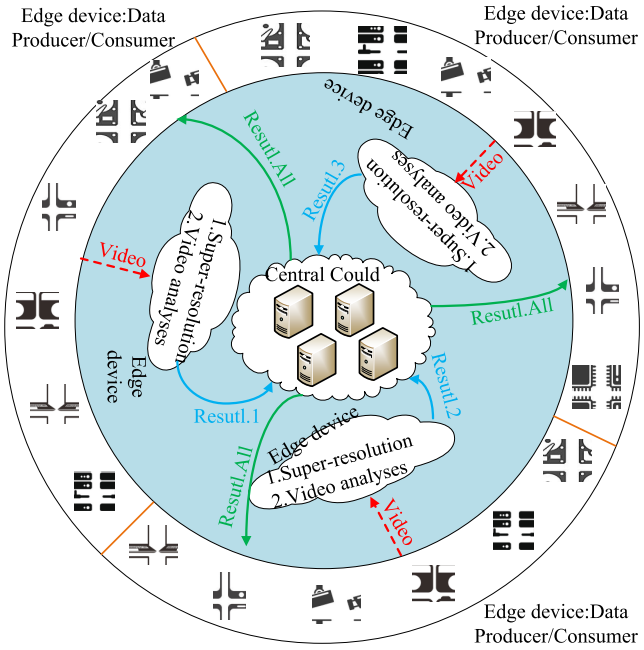

FIGURE 1. The architecture of edge computing for video analytics.

by producing additional details from LR images. Multiframe-based methods achieve good performance with small magnification factor. However, these methods suffer from large magnification factor.

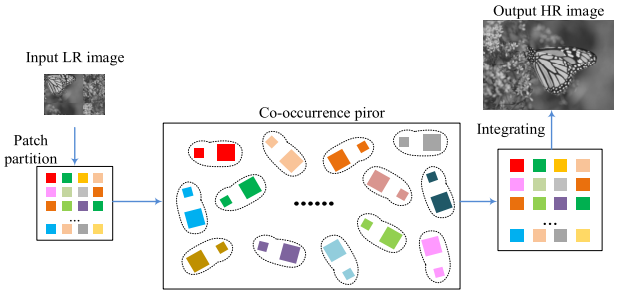

FIGURE 2. The flowchart of learning-based SR methods.

Learning-based SR methods estimate mapping relationships between LR images and HR images [6]–[18]. These methods are shown in Fig. 2. Learning-based methods can be further classified into three types according to mapping relationship estimation approaches, i.e., regression-based methods [10], [11], neighbor embedding (NE)-based methods [7], [8] and sparse coding (SC)-based methods [13]–[21]. The regression-based methods use complicated statistical models to predict the mapping relationship. Dai *et al.* proposed jointly optimized regressors (JOR) method dividing patches into multiple clusters to estimate mapping relationships [11]. However, the estimated relationships are not always accurate.The NE-based methods estimate the HR patch with the information of its nearest HR patches. Locally linear embedding (LLE) is applied to deal with SR tasks in [7]. The assumption of LLE is that each patch and its neighbors are locally linear in manifold.

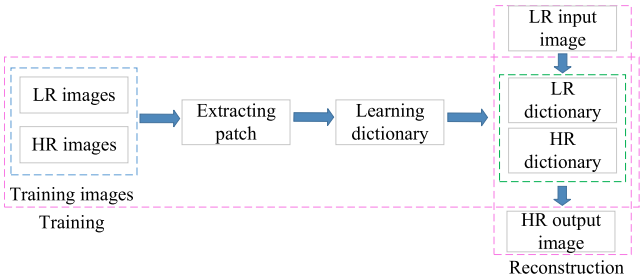

FIGURE 3. The flowchart of SC-based SR methods.

The SC-based methods work well under condition that an image can be sparsely represented based on an over-complete dictionary [13]–[15]. These methods are illustrated in Fig. 3. Yang *et al.* assumed that sparse coefficient of an LR patch is same with that of its corresponding HR patch [13]. The sparse coefficient can be used to reconstruct the HR patch with HR dictionary. Later, Zeyde *et al.* improved Yang's algorithm by employing principal component analysis (PCA) and orthogonal matching pursuit (OMP) algorithms [15]. Wang *et al.* proposed a semi-coupled dictionary learning (SCDL) method [16]. With only one pair of HR and LR dictionaries, it is difficult to represent various patterns in images.

Generally, the existing SC-based SR methods typically suffer from the following two problems. 1) It is too strict if the sparse coefficient of an LR patch is supposed to be the same as its HR version; and 2) Using one pair of HR and LR dictionaries to represent various patterns in images is unreasonable.

Inspired by JOR [11] and based on SCDL [16], in this work, we propose to overcome the two problems and finally achieve better SR performance. To relax the strict assumption, we suppose that the sparse coefficient of an LR patch is linearly related to that of its corresponding HR patch. To accurately represent different patterns in images, multiple pairs of dictionaries are jointly learned. Thus each pair of dictionaries provides more accurate sparse representation.

II. RELATED WORK

A. SC-BASED SR METHODS

Fig. 4 illustrates the flowchart of SC-based SR methods.

1) TRAINING PHASE

Given an HR image I_h, its down-sampled and blurred version is I_l.

$$I_l = HBI_h \tag{1}$$

where H and B are down-sampling and blurring operations, respectively.

a: EXTRACTING PATCH

Given LR image I_l, y^i refers to a patch extracted from I_l.

$$y^i = Patch_L^i(I_l) \tag{2}$$

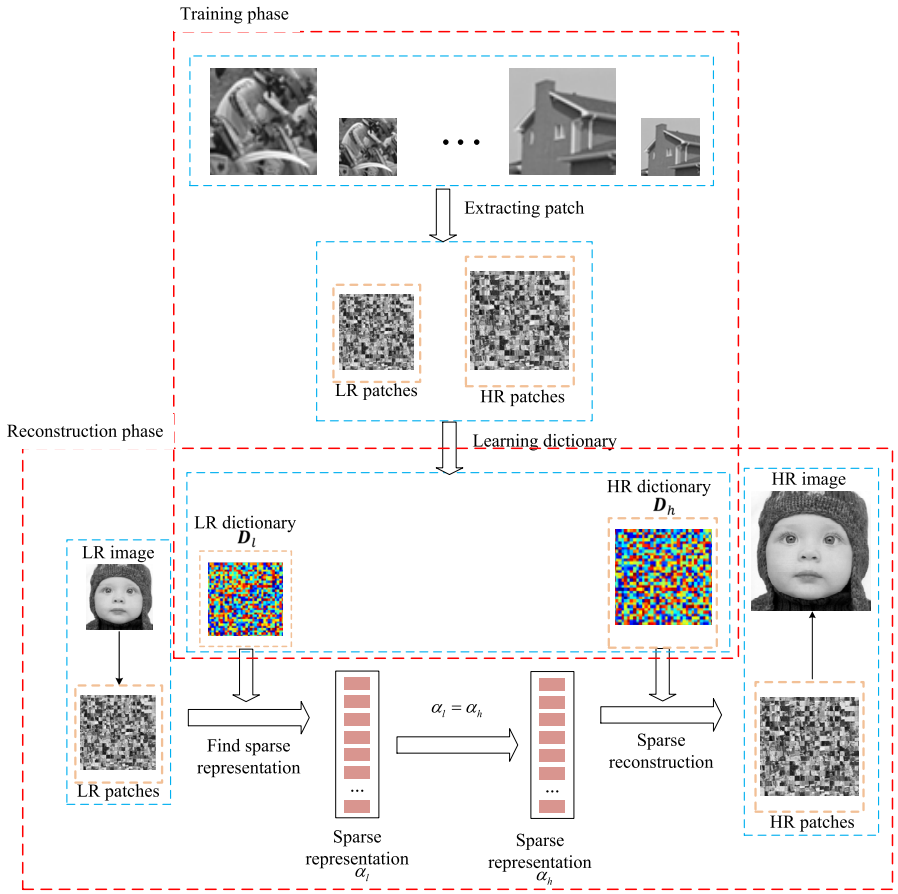

FIGURE 4. The implementation of SC-based methods.

where $Patch_L^i(.)$ is an extracting patch operator for LR image I_l. The size of y^i is $\sqrt{n} \times \sqrt{n}$.

Then, the corresponding HR patch x^i is extracted from HR image I_h. The size of x^i is $\sqrt{nL} \times \sqrt{nL}$.

$$x^i = Patch_H^i(I_h) \tag{3}$$

where $Patch_H^i(\cdot)$ is an extracting operator for HR image I_h.

b: LEARNING DICTIONARY

Evidently, sparse coefficient is a connection between LR patch and its corresponding HR patch. Sparse coding based methods assume that the sparse coefficient of LR patch is same as that of its corresponding LR patch. The following optimization problem should be solved:

$$\min_{\{D_h, D_l, \alpha\}} \|X - D_h\alpha\|_2 + \|Y - D_l\alpha\|_2 + \lambda \|\alpha\|_1 \tag{4}$$

where $D_l \in \Re^{n \times z}$ and $D_h \in \Re^{nL \times z}$ are dictionaries. D_l and D_h can be achieved by the following procedures:

Step 1: Initial D_l and corresponding D_h as random matrix.

Step 2: Fix D_l and D_h, update α by

$$\alpha = \arg\min(\|X - D_h\alpha\|_2 + \frac{1}{n}\|Y - D_l\alpha\|_2 + \lambda \|\alpha\|_1). \tag{5}$$

Step 3: Fix α, update D_l and D_h by

$$\{D_l, D_h\} = \arg\min_{D_l, D_h} \|X - D_h\alpha\| + \|Y - D_l\alpha\|. \tag{6}$$

Step 4: Repeat Step2 and Step3 until convergence.

2) RECONSTRUCTION PHASE

For a given LR image Y_{test}, we can obtain its patches $\{y_{test}^i\}$ as Eq. (2). We obtain the sparse coefficient $\hat{\alpha}_l^i$

$$\hat{\alpha}_l^i = \arg\min_{\hat{\alpha}_l^i} \sum_{i=1}^{P} \left\| D_l\hat{\alpha}_l^i - y_{test}^i \right\|_2 + \lambda \left\| \hat{\alpha}_l^i \right\|_0. \tag{7}$$

Then, we can reconstruct HR patches as:

$$\hat{x}^i = D_h\hat{\alpha}_l^i. \tag{8}$$

All HR patches $\hat{x}^i$ are merged to achieved the reconstruction HR image $\hat{X}$.

B. SCDL METHODS

It is too strict if the sparse coefficient of an LR patch is supposed to be the same as its HR version. To relax the strict assumption, we suppose that the sparse coefficient of

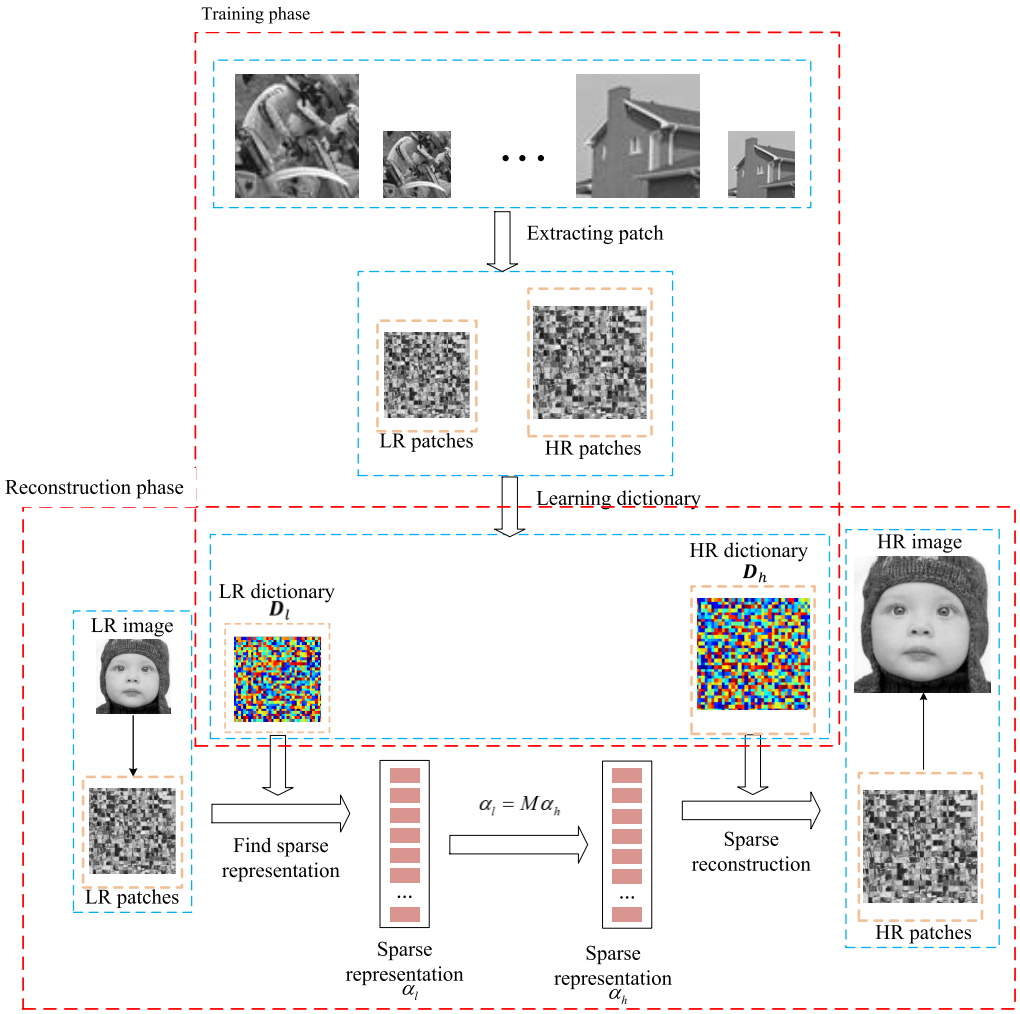

FIGURE 5. The implementation of SCDL methods.

an LR patch is linearly related to that of its corresponding HR patch [16], as

$$\alpha_l = M\alpha_h, \tag{9}$$

where M is the linear projection.

Therefore, the optimization problem becomes

$$\min_{\{D_h, D_l, M, \alpha_l, \alpha_h\}} \|X - D_h\alpha_h\|_2 + \|Y - D_l\alpha_l\|_2 + \lambda_l \|\alpha_l\|_1 + \lambda_h \|\alpha_h\|_1 + \lambda_M \|M\|_1, \tag{10}$$

D_l, D_h, α_l, α_h and M can be obtained through Algorithm 1. The implementation of SCDL methods is illustrated in Fig. 5.

III. PROPOSED METHOD

Inspired by JOR [11] and based on SCDL [16], in this work, to relax the strict assumption, we suppose that the sparse coefficient of an LR patch is linearly related to that of its corresponding HR patch. To accurately represent different patterns in images, multiple pairs of dictionaries are jointly learned. Thus each pair of dictionaries can provide more accurate sparse representation.

Algorithm 1

Step1: Initial D_l and D_h, as random matrix. M can be initialized as identity matrix I.

Step2: Fix D_l, D_h and M, update α_l, α_h by

$$\{\alpha_h, \alpha_l\} = \arg\min(\|X - D_h\alpha_h\|_2 + \|Y - D_l\alpha_l\|_2). \tag{11}$$

Eq. (11) can be solved by LARS [16].

Step3: Fix α_l and α_h, and update D_l and D_h by

$$\{D_l, D_h\} = \arg\min_{D_l, D_h} \left\|x^i - D_h\alpha_h\right\| + \left\|y^i - D_l\alpha_l\right\|. \tag{12}$$

Step4: With dictionaries D_l, D_h fixed, the linear projection M can be updated as:

$$M = \arg\min(\|\alpha_l - M\alpha_h\|_2 + (\lambda_M/\gamma)\|M\|) \tag{13}$$

A. JOINT LEARNING DICTIONARIES

Given that the patches are diverse in the patch space, using one pair of HR and LR dictionaries to represent various

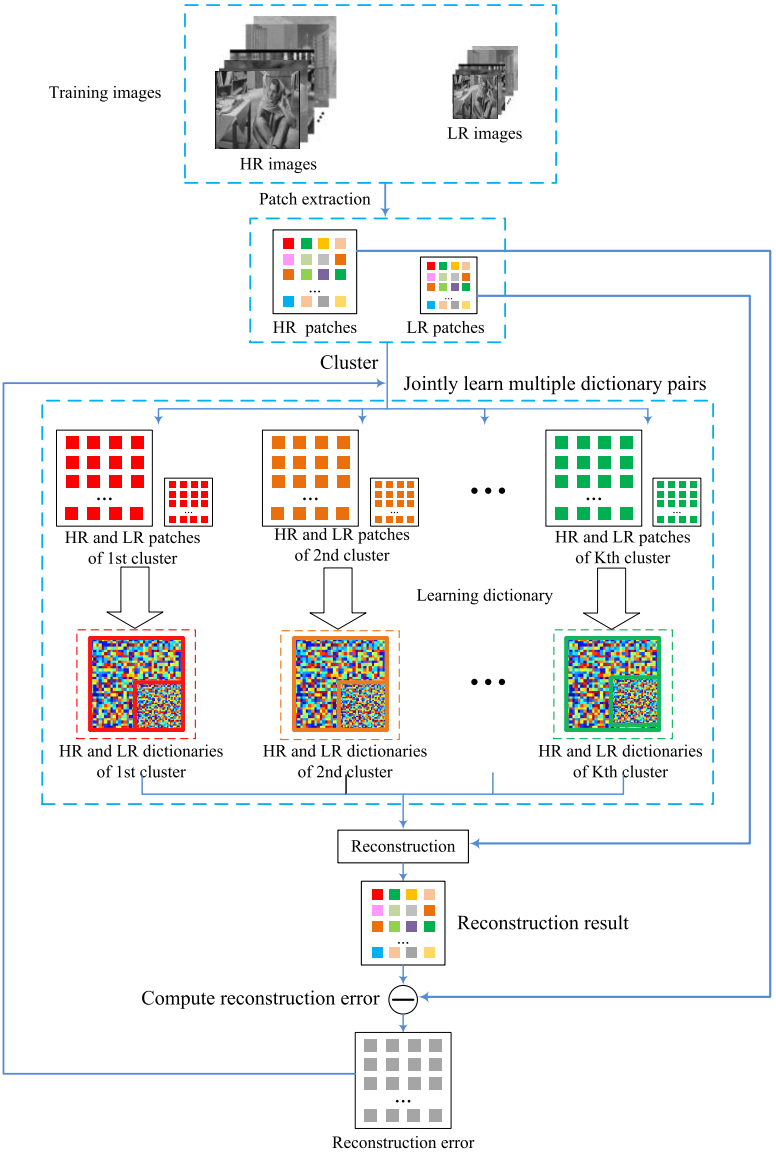

FIGURE 6. The implementation of joint dictionary learning.

patterns in images is unreasonable. We group the patches into n clusters. Dictionaries are learned for each cluster. These HR and LR dictionary pair can precisely reconstruct the patches in each cluster.

We minimize the following function

$$\arg\min_{C} \sum_{i=1}^{N} \sum_{k=1}^{K} c_{k,i} \left\| D_{h,k}\alpha_{h,k}^{i} - x^{i} \right\|^{2}, \tag{14}$$

where C is an $N \times K$ matrix with elements $c_{k,j}$ indicating that x^i is identified to a cluster k for $c_{k,j} = 1$ and is not classified to k for $c_{k,j} = 0$. The term $\alpha_{l,k}^{i}$ is the sparse coefficient of y^i according to k^{th} HR dictionary $D_{h,k}$.

Multiple dictionary pairs are learned as Algorithm 2. The methods are illustrated in Fig. 6.

Algorithm 2

Step 1. Initialization

All patches are partitioned into K clusters K-means.

Step 2. Sparse coding phase of multiple dictionaries

(1) We learn multiple dictionaries $\{D_{h,k}, D_{l,k}\}$ based on Algorithm 1.

(2) With $D_{h,k}$ minimizing the error for sparse representation, we update the cluster k, to which y^i is identified, as

$$k = \arg\min_{k} \left\| D_{h,k}\alpha_{l,k}^{i} - x^{i} \right\|_{2}. \tag{15}$$

(3) Repeat (1) and (2), and Step 2 is done when

$$\sum_{i=1}^{N} \sum_{k=1}^{K} c_{k,i} \left\| D_{h,k}\alpha_{l,k}^{i} - x^{i} \right\|^{2} \leq \varepsilon. \tag{16}$$

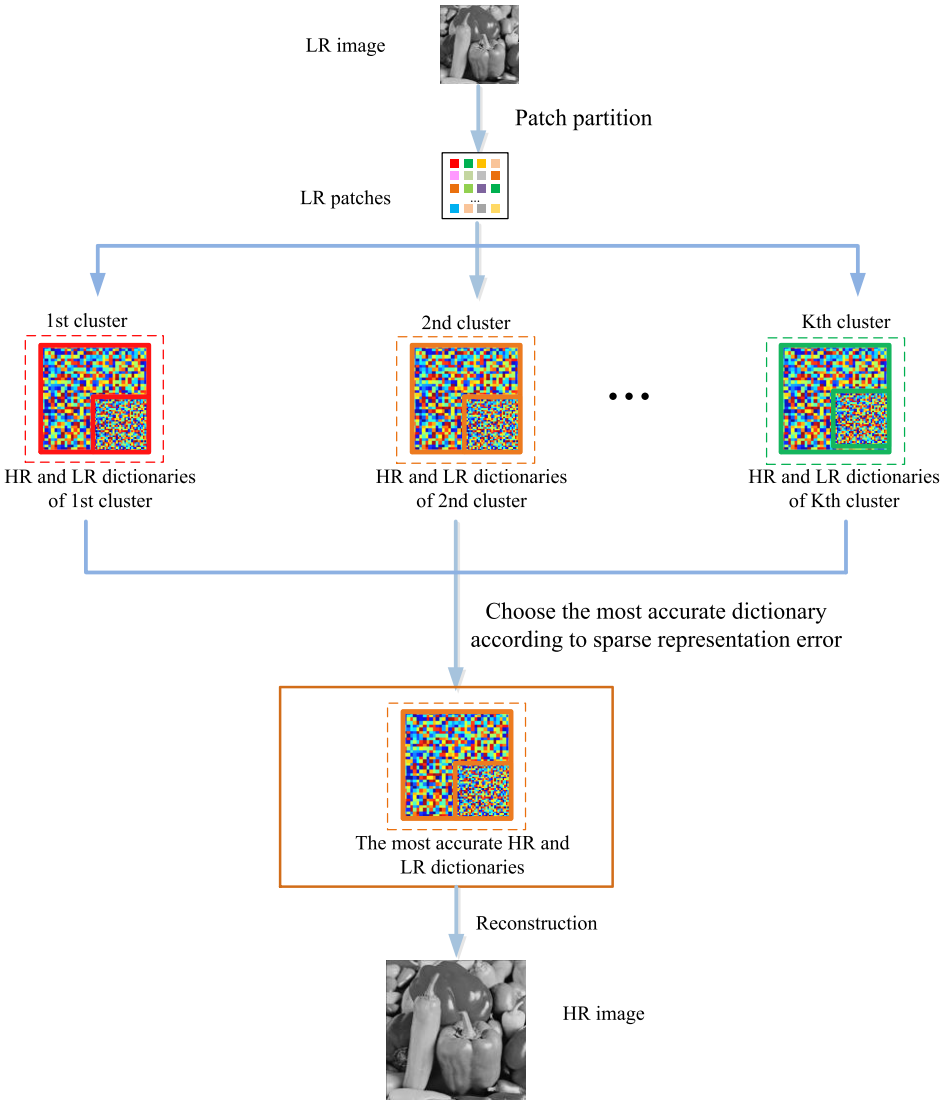

FIGURE 7. The implementation of reconstruction.

B. HR IMAGE RECONSTRUCTION

Sparse coefficient $\alpha_i^{l,k}$ and the sparse representation error e_k can be obtained as:

$$\alpha_i^{l,k} = \arg\min_{\alpha_i^{l,k}} \left\| D_{l,k}\alpha_i^{l,k} - y_{test}^i \right\|_2 + \lambda \left\| \alpha_i^{l,k} \right\|_0 \quad (17)$$

$$e_k = \left\| y_{test}^i - D_{l,k}\alpha_i^{l,k} \right\|_2 \quad (18)$$

where e_k is the error of sparse representation for $\{D_{h,k}, D_{l,k}\}$. Smaller e_k indicates that the dictionary pair can represent more accurately.

We reconstruct the HR patch according to $D_{h,m}$ which can get the smallest sparse representation error e_m.

$$x^{m,i} = D_{h,m}\alpha_l^{i,m} \quad (19)$$

HR image reconstruction is illustrated as Fig. 7.

TABLE 1. The parameters of our experiment.

Parameters	Value
Upscaling factor	3
Patch size	3*3
Overlap for patch	2
Dictionary size	5000
The number of clusters	12
The number of document patches extracted from the training set in the learning stage	10000

IV. PROPOSED METHOD

A. SAMPLES AND SETTINGS

The training set is same as [13] containing 91 images. For testing, Set 5 and Set 14 datasets which are typically employed. Fig. 8 shows the part of test images.

Parameters for our method are illustrated as Table 1.

B. COMPARISON WITH STATE-OF-THE-ART ALGORITHMS

The proposed method is compared with some SR methods, namely, cubic B-spline interpolation, Yang's [13], Zeyde's [15] and SCDL [16].

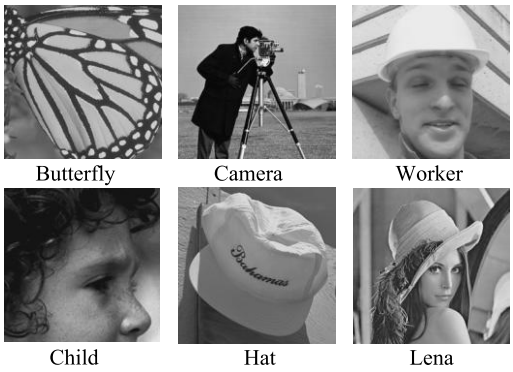

FIGURE 8. Part of test images.

TABLE 2. Numerical results of Figs. 9–14.

	Cubic B-spline	Yang's method	Zyede's method	SCDL method	Our method
	PSNR	PSNR	PSNR	PSNR	PSNR
	SSIM	SSIM	SSIM	SSIM	SSIM
Butterfly	22.26	22.32	22.38	24.52	**24.70**
	0.7640	0.7854	0.7914	0.8574	**0.8637**
Cameraman	21.66	22.47	22.61	22.69	**22.85**
	0.6917	0.6957	0.6977	0.7477	**0.7512**
Worker	29.65	30.37	30.53	33.35	**33.87**
	0.8481	0.8390	0.8497	0.8913	**0.8952**
Child	29.97	30.68	30.77	31.88	**31.91**
	0.7093	0.7166	0.7181	0.7475	**0.7487**
Hat	27.47	28.33	28.46	28.99	**29.22**
	0.7649	0.7638	0.7735	0.8090	**0.8151**
Lena	22.85	23.84	23.96	24.63	**24.77**
	0.6788	0.6977	0.6987	0.7949	**0.7984**

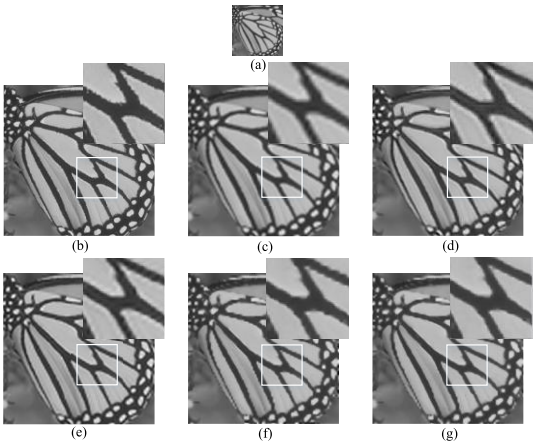

FIGURE 9. Experimental results of image butterfly: (a) LR image, (b) ground-truth (c) r Cubic B-spline, (d) Yang's, (e) Zeyde's, (f) SCDL and (g) Our method.

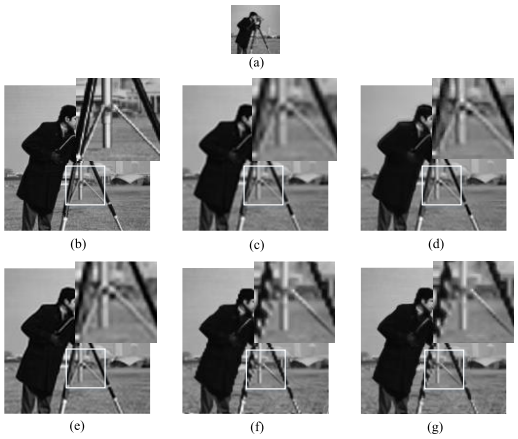

FIGURE 10. Experimental results of image Cameraman: (a) LR image, (b) ground-truth (c) r Cubic B-spline, (d) Yang's, (e) Zeyde's, (f) SCDL and (g) Our method.

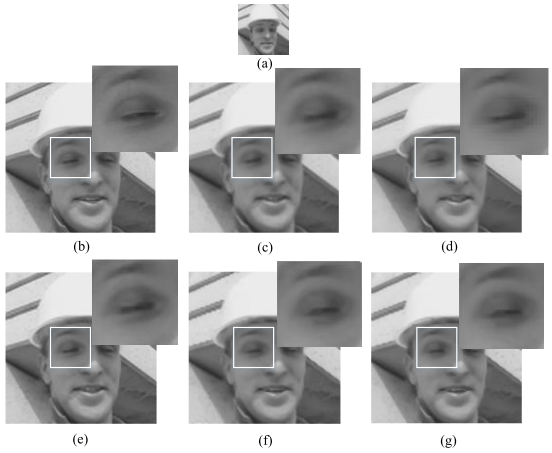

FIGURE 11. Experimental results of image Worker: (a) LR image, (b) ground-truth (c) r Cubic B-spline, (d) Yang's, (e) Zeyde's, (f) SCDL and (g) Our method.

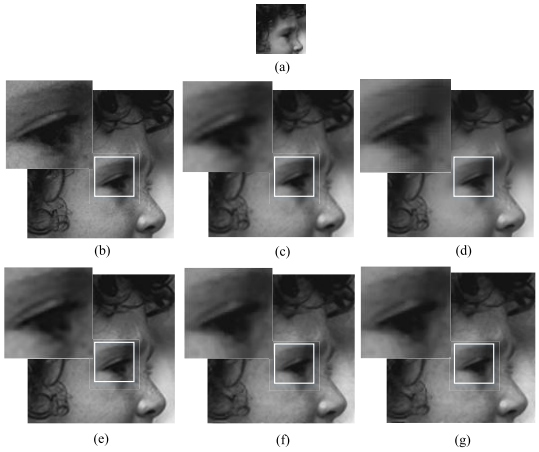

FIGURE 12. Experimental results of image Child: (a) LR image, (b) ground-truth (c) r Cubic B-spline, (d) Yang's, (e) Zeyde's, (f) SCDL and (g) Our method.

The visual quality of the results are shown in Figs. 9–14. By observing the details of reconstructed results, we can see numerous sharpness edges and artifacts in the reconstructed images by cubic B-spline interpolation method. Yang's method and Zeyde's method recover many details. However, numerous obvious zigzagging effects are

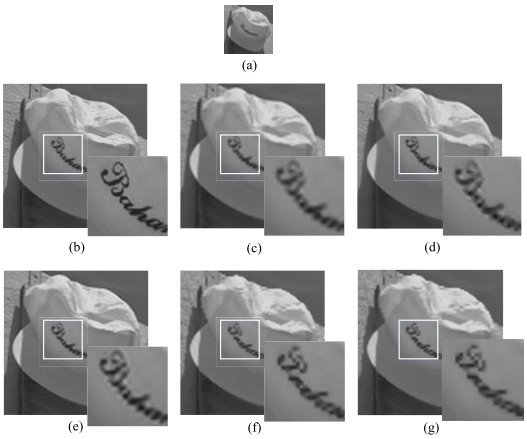

FIGURE 13. Experimental results of image Hat: (a) LR image, (b) ground-truth (c) r Cubic B-spline, (d) Yang's, (e) Zeyde's, (f) SCDL and (g) Our method.

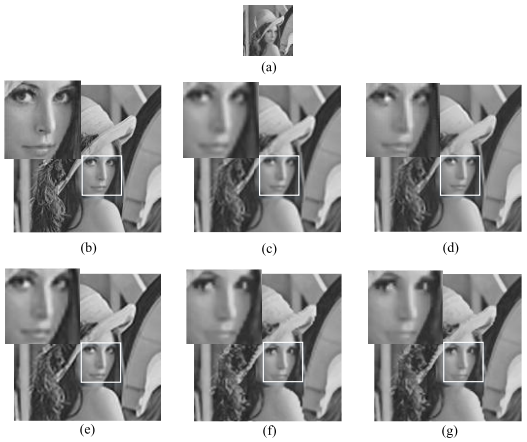

FIGURE 14. Experimental results of image Lena: (a) LR image, (b) ground-truth (c) r Cubic B-spline, (d) Yang's, (e) Zeyde's, (f) SCDL and (g) Our method.

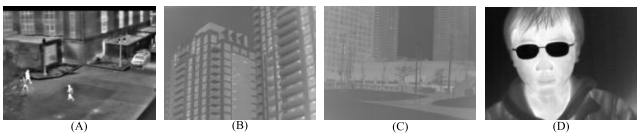

FIGURE 15. IR images.

found at the edges. SCDL method performs well in generating rich details and sharp edges, but several resulted images appear unnatural in certain parts. By contrast, the proposed method leads the best visual quality. The approach not only reconstructs a large number of shaper edges but also recovers highly clear texture. The PSNR and SSIM values of the SR results on LR images obtained using various methods are listed in Table 2. We can observe that the proposed method achieve highest PSNR and SSIM among those of other methods.

C. EXPERIMENTAL RESULTS FOR IR IMAGES

Infrared images are employed to further verify the effectiveness of the proposed method. The IR images are downloaded from http://www.dgp.toronto.edu/~nmorris/data/IRData/ and IRIS Thermal/Visible Face Database. Fig. 15 shows the samples of the test images.

Figs. 16–19 shows the results of difierent methods for the IR image. We can see that Yang's method and Zeyde's method can recovering numerous image details. However, they produce some jagged artifacts at the edges. Although SCDL method reconstruct more details, it still bring some ringing artifacts. Our method can recover the sharp edges, and

TABLE 3. Numerical results of Figs. 16–19.

	Cubic B-spline	Yang's method	Zyede's method	SCDL method	Our method
	PSNR	PSNR	PSNR	PSNR	PSNR
	SSIM	SSIM	SSIM	SSIM	SSIM
A	23.44	25.42	25.47	25.56	**25.62**
	0.7337	0.7551	0.7609	0.8269	**0.8321**
B	37.80	39.83	39.90	40.05	**40.12**
	0.3687	0.3703	0.3707	0.3712	**0.3727**
C	38.80	39.83	39.90	40.05	**40.09**
	0.5983	0.6174	0.6183	0.6841	**0.6891**
D	32.86	33.25	33.46	33.67	**33.96**
	0.8957	0.9084	0.9143	0.9162	**0.9186**

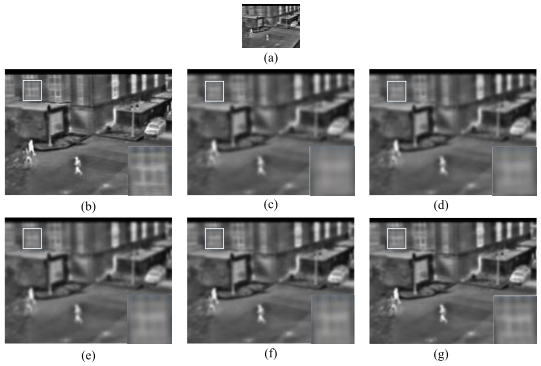

FIGURE 16. Experimental results of image A: (a) LR image, (b) ground-truth (c) r Cubic B-spline, (d) Yang's, (e) Zeyde's, (f) SCDL and (g) Our method.

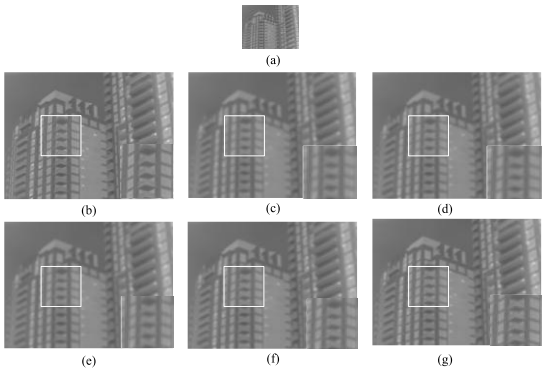

FIGURE 17. Experimental results of image B: (a) LR image, (b) ground-truth (c) r Cubic B-spline, (d) Yang's, (e) Zeyde's, (f) SCDL and (g) Our method.

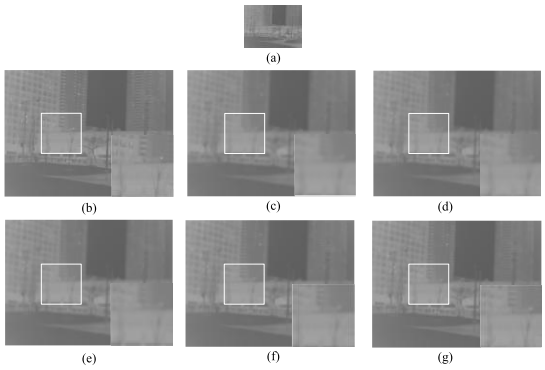

FIGURE 18. Experimental results of image C: (a) LR image, (b) ground-truth (c) r Cubic B-spline, (d) Yang's, (e) Zeyde's, (f) SCDL and (g) Our method.

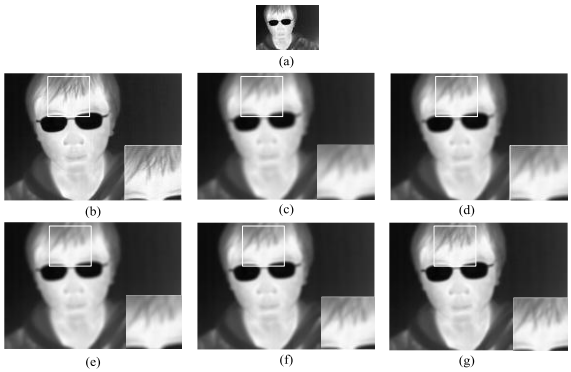

FIGURE 19. Experimental results of image D: (a) LR image, (b) ground-truth (c) r Cubic B-spline, (d) Yang's, (e) Zeyde's, (f) SCDL and (g) Our method.

contains fewer artifacts. In Table 3, the PSNRs and SSIMs of the reconstructed SR images are listed, and we see the proposed method is better.

V. CONCLUSION

In this study, by assuming the sparse coefficient of an HR patch is linearly related to that of an LR patch, we partition training patches into multiple clusters through joint learning multiple dictionary pairs. Then, for all the training patches, multiple pairs of dictionaries with the least SR errors are generated. Experiments demonstrate that, compared with the state-of-the-art methods, the proposed achieves competitive performance.

REFERENCES

[1] R. Kimmel, "Demosaicing: Image reconstruction from color CCD samples," *IEEE Trans. Image Process.*, vol. 8, no. 9, pp. 1221–1228, Sep. 1999.
[2] X. Li, "Demosaicing by successive approximation," *IEEE Trans. Image Process.*, vol. 14, no. 3, pp. 370–379, Mar. 2005.
[3] H. Shen, L. Zhang, B. Huang, and P. Li, "A MAP approach for joint motion estimation, segmentation, and super resolution," *IEEE Trans. Image Process.*, vol. 16, no. 2, pp. 479–490, Feb. 2007.
[4] L. Zhang, H. Zhang, H. Shen, and P. Li, "A super-resolution reconstruction algorithm for surveillance images," *Signal Process.*, vol. 90, no. 3, pp. 848–859, 2010.
[5] S. Farsiu, M. D. Robinson, M. Elad, and P. Milanfar, "Fast and robust multiframe super resolution," *IEEE Trans. Image Process.*, vol. 13, no. 10, pp. 1327–1344, Oct. 2004.
[6] W. T. Freeman, T. R. Jones, and E. C. Pasztor, "Example-based super-resolution," *IEEE Comput. Graph. Appl.*, vol. 22, no. 2, pp. 56–65, Mar./Apr. 2002.
[7] H. Chang, D.-Y. Yeung, and Y. Xiong, "Super-resolution through neighbor embedding," in *Proc. CVPR*, Washington, DC, USA, Jun. 2004, pp. 275–282.
[8] K. Zhang, X. Gao, X. Li, and D. Tao, "Partially supervised neighbor embedding for example-based image super-resolution," *IEEE J. Sel. Topics Signal Process.*, vol. 5, no. 2, pp. 230–239, Apr. 2011.
[9] X. Yang, W. Wu, K. Liu, K. Zhou, and B. Yan, "Fast multisensor infrared image super-resolution scheme with multiple regression models," *J. Syst. Archit.*, vol. 64, pp. 11–25, Mar. 2016.
[10] W. Wu, Z. Liu, and X. He, "Learning-based super resolution using kernel partial least squares," *Image Vis. Comput.*, vol. 29, no. 6, pp. 394–406, 2011.
[11] D. Dai, R. Timofte, and L. Van Gool, "Jointly optimized regressors for image super-resolution," *Comput. Graph. Forum*, vol. 34, no. 2, pp. 95–104, 2015.
[12] M. Aharon, M. Elad, and A. Bruckstein, "K-SVD: An algorithm for designing overcomplete dictionaries for sparse representation," *IEEE Trans. Signal Process.*, vol. 54, no. 11, pp. 4311–4322, Nov. 2006.
[13] J. Yang, J. Wright, T. S. Huang, and Y. Ma, "Image super-resolution via sparse representation," *IEEE Trans. Image Process.*, vol. 19, no. 11, pp. 2861–2873, Nov. 2010.
[14] S. Y. Yang, Z. Z. Liu, and L. C. Jiao, "Multitask dictionary learning and sparse representation based single-image super-resolution reconstruction," *Neurocomputing*, vol. 74, no. 17, pp. 3193–3203, 2011.
[15] R. Zeyde, M. Elad, and M. Protter, "On single image scale-up using sparse-representations," in *Proc. 7th Int. Conf. Curves Surfaces*, Berlin, Germany, 2012, pp. 711–730.
[16] S. Wang, L. Zhang, Y. Liang, and Q. Pan, "Semi-coupled dictionary learning with applications to image super-resolution and photo-sketch synthesis," in *Proc. CVPR*, Providence, RI, USA, 2012, pp. 2216–2223.
[17] G. Jeon, M. Anisetti, D. Kim, V. Bellandi, E. Damiani, and J. Jeong, "Fuzzy rough sets hybrid scheme for motion and scene complexity adaptive deinterlacing," *Image Vis. Comput.*, vol. 27, no. 4, pp. 425–436, 2009.
[18] X. Chen, L. He, G. Jeon, and J. Jeong, "Multidirectional weighted interpolation and refinement method for Bayer pattern CFA demosaicking," *IEEE Trans. Circuits Syst. Video Technol.*, vol. 25, no. 8, pp. 1271–1282, Aug. 2015.
[19] G. Jeon, M. Anisetti, and S. H. Kang, "A rank-ordered marginal filter for deinterlacing," *Sensors*, vol. 13, no. 3, pp. 3056–3065, 2013.
[20] X. Yang, W. Wu, K. Liu, W. Chen, P. Zhang, and Z. Zhou, "Multi-sensor image super-resolution with fuzzy cluster by using multi-scale and multi-view sparse coding for infrared image," *Multimed Tools Appl.*, vol. 76, no. 23, pp. 24871–24902, 2017, doi: https://doi.org/10.1007/s11042-017-4639-4.
[21] W. Wu, X. Yang, K. Liu, Y. Liu, and B. Yan, "A new framework for remote sensing image super-resolution: Sparse representation-based method by processing dictionaries with multi-type features," *J. Syst. Archit.*, vol. 64, pp. 63–75, Mar. 2016.
[22] X. Yang, W. Wu, K. Liu, W. Chen, and Z. Zhou, "Multiple dictionary pairs learning and sparse representation-based infrared image super-resolution with improved fuzzy clustering," *Soft Comput.*, 2017, doi: https://doi.org/10.1007/s00500-017-2812-3.

XIAOMIN YANG received the B.S. degree and the Ph.D. degree in communication and information system from Sichuan University in 2002 and 2007, respectively. She held a post-doctoral position with the University of Adelaide. She is currently an Associate Professor with the College of Electronics and Information Engineering, Sichuan University. Her research interests are image processing and pattern recognition.

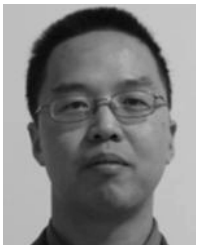

WEI WU received the B.S. degree from Tianjin University, and the M.S. and Ph.D. degrees in communication and information system from Sichuan University. He held a post-doctoral position with the National Research Council Canada. He is currently a Professor with the College of Electronics and Information Engineering, Sichuan University. His research interests are image processing and pattern recognition.

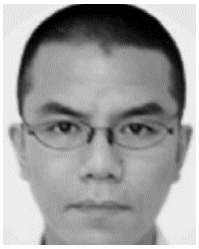

KAI LIU received the B.S. degree from Sichuan University, and the Ph.D. degree from the University of Kentucky. He is currently a Professor with the College of Electrical Engineering and Information, Sichuan University.

PYOUNG WON KIM is currently an Associate Professor with the Department of Korea Language Education, Incheon National University, Incheon, South Korea.

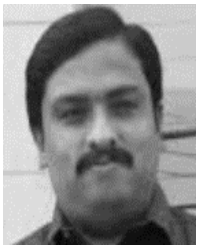

ARUN KUMAR SANGAIAH is currently a Professor with the School of Computing Science and Engineering, VIT University, India.

GWANGGIL JEON received the B.S., M.S., and Ph.D. (*summa cum laude*) degrees from the Department of Electronics and Computer Engineering, Hanyang University, Seoul, South Korea, in 2003, 2005, and 2008, respectively. From 2008 to 2009, he was with the Department of Electronics and Computer Engineering, Hanyang University, from 2009 to 2011, he was with the School of Information Technology and Engineering, University of Ottawa, as a Post-Doctoral Fellow, and from 2011 to 2012, he was with the Graduate School of Science and Technology, Niigata University, as an Assistant Professor. He is currently an Assistant Professor with the Department of Embedded Systems Engineering, Incheon National University, Incheon, South Korea. His research interests fall under the umbrella of image processing, particularly image compression, motion estimation, demosaicking, and image enhancement as well as computational intelligence, such as fuzzy and rough sets theories. He was a recipient of the IEEE Chester Sall Award in 2007 and the 2008 ETRI Journal Paper Award.